DALTON
COMMUNICATION

Hydrothermal synthesis of two-dimensional organic–inorganic hybrid materials of the nickel–molybdate family: the structures of [{Ni(3,3′-bpy)$_2$}$_2$Mo$_4$O$_{14}$] and [Ni(3,3′-Hbpy)Mo$_4$O$_{13}$(OH)]

Robert L. LaDuca, Jr.,*[a] **Matthew Desciak,**[a] **Matthew Laskoski,**[a] **Randy S. Rarig, Jr.**[b] **and Jon Zubieta***[b]

[a] *Department of Chemistry and Physics, King's College, Wilkes-Barre, PA 18711, USA*
[b] *Department of Chemistry, Syracuse University, Syracuse, NY 13244, USA*

Received 12th February 2000, Accepted 7th June 2000
Published on the Web 30th June 2000

The hydrothermal chemistry of the Ni(II)/molybdate/3,3′-bipyridine system exhibits pronounced pH dependence, such that under basic conditions a 2-D material with embedded clusters [{Ni(3,3′-bpy)$_2$}$_2$Mo$_4$O$_{14}$] 1 is observed, while under acidic conditions the 2-D bimetallic oxide network of [Ni(3,3′-Hbpy)Mo$_4$O$_{13}$(OH)] 2 is isolated.

The extensive contemporary activity in solid state inorganic oxides derives from their vast compositional range and diverse structural chemistry which endows these materials with physical properties with applications to sorption, catalysis, electrical conductivity and solar energy conversion.[1,2] The discovery of new materials of this class is driven by synthesis; albeit rational design of such solids remains an elusive goal.[3] However, one useful strategy for the modification of inorganic oxide substructures exploits organic molecules or ions as structure-directing components of a hybrid material, an approach amply demonstrated in the design of families of materials such as zeolites,[4] mesoporous oxides[5] and oxometal phosphates,[6] as well as Nature's remarkable biomineralized materials.[7,8] Expanding on this approach, we have recently elaborated aspects of the structural chemistry of the copper molybdate family with 4,4′-bipyridine and related tethered 4,4′-bipyridine ligands (NC_5H_4–X–C_5H_4N, X = NH, S, C_2H_2, *etc.*).[9–15] These materials manifest the structural influences both of the coordination preferences of the "secondary" metal site [whether Cu(I) or Cu(II)] and of the ligand geometry and spatial extension. Most significantly, it is observed that the Cu(I)/ligand/molybdate subclass exhibits discrete polymeric coordination complex cations $\{Cu(ligand)\}_n^{n+}$ and molybdate cluster $\{Mo_xO_y\}^{n-}$ substructures, while the Cu(II)/ligand/molybdate subclass is characterized by incorporation of the copper into a copper–molybdenum bimetallic oxide substructure. As an extension of this synthetic approach to oxides, we have begun to investigate the consequences of ligand geometry on the oxide substructure, specifically structural modifications which may occur concomitantly to changes in donor group orientations. In addition, we have sought to exploit the more regular and predictable octahedral geometry of Ni(II) as the charge compensating secondary metal site. As part of these studies, the linear 4,4′-bipyridine component has been replaced by the angular donor 3,3′-bipyridine (3,3′-bpy) in the preparation of members of the nickel–molybdate subclass, now represented by two novel 2-D oxides, [{Ni(3,3′-bpy)$_2$}$_2$Mo$_4$O$_{14}$] **1** and [Ni(3,3′-Hbpy)Mo$_4$O$_{13}$(OH)] **2**.

Compound **1** was prepared in 60% yield as dark blue needles in the hydrothermal reaction of $NiCl_2\cdot 6H_2O$, MoO_3, 3,3′-bpy and H_2O under basic conditions in the mole ratio 1.02 : 1.00 : 2.02 : 1510 for 2 d at 120 °C.† In contrast, compound **2** was synthesized in 30% yield of dark green crystals in the hydrothermal reaction of $NiCl_2\cdot 6H_2O$, MoO_3, 3,3′-bpy and H_2O under acidic conditions in the mole ratio 1.37 : 1.27 : 1.00 : 1181 for 3 d at 180 °C. The IR spectra of both **1** and **2** exhibit several bands in the 890–940 cm^{-1} range attributed to ν(Mo=O) and a series of bands between 1100 and 1500 cm^{-1} associated with the ligand. The isolation of **1** and **2** demonstrates the critical influence of pH on the identity of products derived from hydrothermal media. In the absence of pH adjustment, only amorphous mixtures of products were observed.

As shown in Fig. 1, the structure of **1** ‡ consists of a layered covalent network constructed from a two-dimensional $\{Ni(3,3'\text{-}bpy)_2\}_n^{2n+}$ grid with $\{Mo_4O_{14}\}^{4-}$ clusters occupying the intralamellar cavities. Alternatively, the structure may be described as a $\{Ni_2Mo_4O_{14}\}$ metal oxide network, with the organic subunits disposed within the cavities and curving into the interlamellar region and providing an organic sheath layering the surfaces of the inorganic networks. The interlayer separation is approximately 9.1 Å.

The Ni(II) coordination geometry is defined by four nitrogen donors from four 3,3′-bpy ligands in the equatorial plane and two oxygen donors, one from each of two adjacent $\{Mo_4O_{14}\}^{4-}$ clusters, in the axial positions. Each 3,3′-bpy ligand bridges to a neighboring Ni(II) site, so that each $\{Ni(3,3'\text{-}bpy)_4\}^{2+}$ grouping links to four adjacent Ni(II) centers. The non-linear orientation of the ligand donor groups serves to generate cavities of circular profile, which accommodate the molybdate clusters. The tetramolybdate subunit, which is unprecedented in the polyoxoanion chemistry, as well as in solid state molybdenum oxide chemistry, consists of two $\{MoO_6\}$ octahedra and two $\{MoO_5\}$ distorted trigonal bipyramids in an edge-sharing arrangement. The polyhedral arrangement is quite distinct from that observed for tetravanadate $\{V_4O_{12}\}^{4-}$ which consists of corner-sharing tetrahedra and does not exhibit the central oxo-group.[16] Furthermore, $\{Mo_4O_{14}\}^{4-}$ is not a structural subunit of any of the octamolybdate $\{Mo_8O_{26}\}^{4-}$ isomers. Four terminal oxo-groups of the cluster are covalently linked to four neighboring Ni(II) sites to provide the 2-D metal oxide connectivity.

The structure of the acidic phase **2** is dramatically distinct from that of **1**. As shown in Fig. 2, the 2-D structure consists of bimetallic oxide networks $\{NiMo_4O_{13}(OH)\}_n^{n-}$ with monodentate and protonated 3,3-Hbpy$^+$ subunits projecting into the interlamellar region. The oxide substructure may be described as a bilayer of edge- and corner-sharing $\{MoO_6\}$ and $\{NiO_5N\}$ octahedra. A network of corner- and edge-sharing $\{MoO_6\}$ octahedra provides a ruffled 2-D substructure with cavities occupied by the Ni(II) centers. Each Ni(II) engages in corner-sharing to four adjacent Mo centers and edge-sharing with two Mo sites. The sixth coordination site of the Ni is occupied by a nitrogen donor of the 3,3-Hbpy$^+$ ligand, which projects into the interlamellar region. The second pyridyl nitrogen of the ligand is protonated and hydrogen-bonded to a doubly-bridging hydroxo group (Mo–OH–Mo) of an adjacent layer. Charge compensation requires that an oxygen site be protonated, and this has been unambiguously identified as the doubly bridging

DOI: 10.1039/b001419m

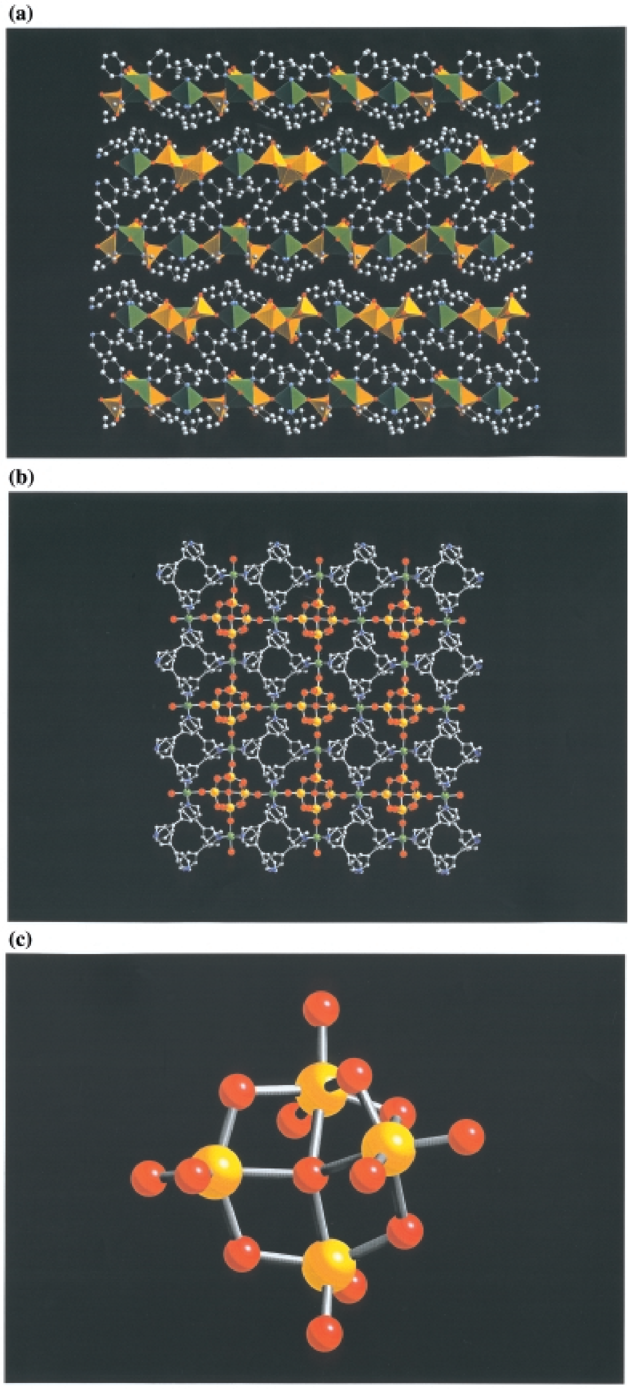

Fig. 1 (a) A view parallel to the crystallographic *b* axis showing the stacking of layers in **1**. (b) A view parallel to the crystallographic *c* axis of **1**, showing the covalent connectivity within the layer. (c) A view of the $\{Mo_4O_{14}\}^{4-}$ cluster imbedded in the network structure of **1**. Selected bond lengths (Å): Mo–O(octahedral sites): 1.745(6) (av.) (×3), 2.218(6) (av.) (×3); Mo–O(trigonal bipyramidal sites): 1.728(5) (av.) (×2), 1.852(5) (av.) (×1); 2.004(5) (av.) (×2); Ni–O, 2.005(5) (av.) (×2); Ni–N, 2.134(5) (av.) (×4).

O14.§ It is noteworthy that in order to achieve this significant hydrogen-bonding interaction between layers, the 3,3-bpy must adopt an *anti*-orientation of the nitrogen atoms, in contrast to the *syn*-orientation found in **1**.

It is instructive to compare the structures of **1** and **2** to those of the nickel molybdate/4,4′-bpy subclass. In common with **1**, the structure of $[\{Ni(H_2O)_2(4,4'\text{-bpy})_2\}_2Mo_8O_{26}]$[10] exhibits a Ni–ligand polymeric substructure with embedded molybdate clusters, providing a 2-D covalent connectivity. However, in contrast to **1**, the 4,4′-bpy material does not possess an extended bimetallic oxide network, but rather $\{Ni_2Mo_8O_{26}\}$ subunits linked through the dipodal ligand. Likewise, the bent

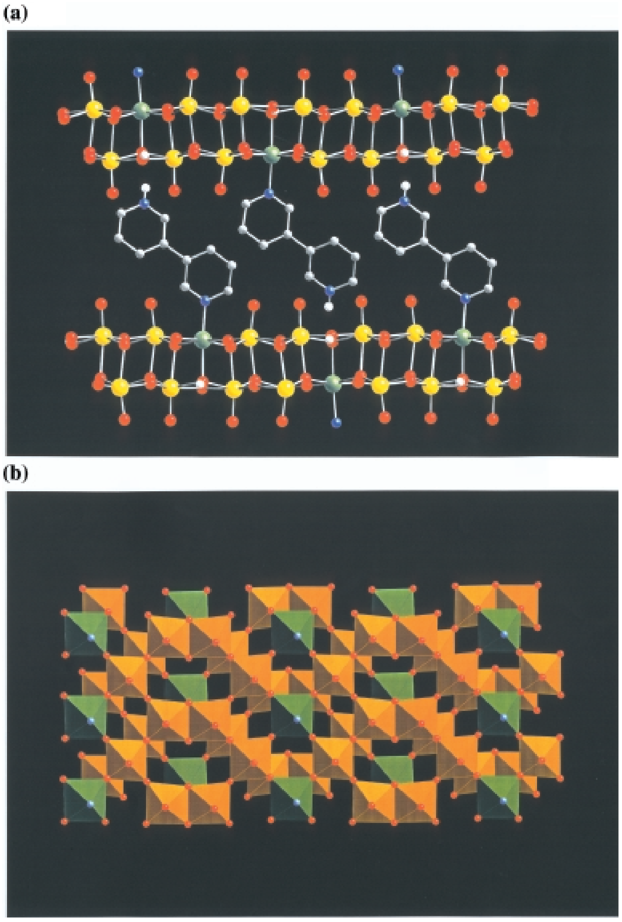

Fig. 2 (a) A view of the stacking of layers in **2**, parallel to the crystallographic *b* axis. The small white spheres represent the hydrogen sites; the yellow spheres are Mo sites and the green are Ni sites. (b) A polyhedral representation of the bimetallic oxide layer of **2**. Selected bond lengths (Å): Mo–O (av.): 1.718(7) (×2), 1.934(7) (×2), 2.266(8) (×2); Ni–O (av.): 2.007(7), Ni–N, 2.045(7).

4,4′-dipyridylamine (dpa) ligand of $[Ni(dpa)_2MoO_4]$[17] produces a 2-D $\{Ni(dpa)_2\}_n^{2n+}$ network, somewhat reminiscent of the nickel–3,3′-bpy network of **1**. However, the steric constraints of the dpa ligand and the donor group orientations prevent formation of large cavities, such that the structure consists of the $\{Ni(dpa)_2\}_n^{2n+}$ networks linked by $\{MoO_4\}^{2-}$ tetrahedra into a 3-D covalently linked framework. These observations confirm that the ligand geometry may be manipulated so as to modify the microstructure of the inorganic oxide component of such composite materials. However, while judicious choice of the secondary metal cation and of the ligand geometry accomplishes the self-assembly of a polymeric cationic substructure and allows a measure of predictability in the isolation of low-dimensional oxide structures, predictability remains problematical as a consequence of the synergism between the organic and inorganic subunits of these materials and of the inherent dynamism of such metastable materials.

Acknowledgements

This work was supported by NSF grant CHE 9987471. The work at King's College was supported by an award from Research Corporation.

Notes and references

† Synthetic details: reactions were carried out in 23 ml Teflon-lined Parr acid digestion bombs. **1**: $NiCl_2\cdot6H_2O$ (0.089 g, 0.375 mmol), MoO_3, (0.053 g, 0.368 mmol), 3,3′-bpy (0.116 g, 0.744 mmol), H_2O (10.0 g, 555.6 mmol); pH adjusted with *ca.* 0.25 mL of 40% Et_4NOH. **2**: $NiCl_2\cdot6H_2O$ (0.154 g, 0.648 mmol), MoO_3 (0.087 g, 0.604 mmol), 3,3′-

bpy (0.074 g, 0.474 mmol), H_2O (10.08 g, 559.7 mmol); pH adjusted with *ca.* 0.25 mL of 1 M HCl.

‡ X-Ray data were collected on a Bruker SMART diffractometer using graphite monochromated Mo-Kα radiation ($\lambda = 0.71073$ Å). Structure solution and refinement were accomplished using the SHELXTL program package (SHELXTL PC™ Siemens Analytical X-ray Instruments, Inc., Madison, WI, 1990). Crystal data: $C_{40}H_{32}Mo_4N_8Ni_2O_{14}$ **1**: orthorhombic, space group $P2_12_12_1$, $\mu = 20.88$ cm^{-1}, $a = 11.3172(5)$, $b = 11.3534(5)$, $c = 33.1523(14)$ Å, $V = 4259.7(3)$ Å^3, $Z = 4$, $D_c = 2.105$ g cm^{-3}, $R1 = 0.0356$, $wR2 = 0.0687$ (10176 reflections). $C_{10}H_{10}Mo_4N_2NiO_{14}$ **2**: orthorhombic, space group $P2_12_12_1$, $\mu = 29.82$ cm^{-1}, $a = 5.541(1)$, $b = 13.737(3)$, $c = 24.134(5)$, $V = 1836.9(7)$ Å^3, $Z = 4$, $D_c = 2.982$ g cm^{-3}, $R1 = 0.0471$, $wR2 = 0.1027$ (4449 reflections).

CCDC reference number 186/2028.

§ The proton is observed as a significant excursion of electron density on the difference Fourier maps. Refinement of positional and isotropic thermal parameters are unexceptional. Furthermore, valence sum calculations[18] clearly indicate that O14 must be the protonation site. The valence sums for all other oxygen atoms of the layer fall in the range 1.83–2.01, while that for O14 in the absence of protonation is 1.26.

1 A. J. Cheetham, *Science*, 1994, **264**, 794 and refs. therein.
2 *Inorganic Materials*, ed. D. W. Bruce and D. O'Hare, Wiley, Chichester, 1992.
3 T. E. Mallouk and H. Lee, *J. Chem. Educ.*, 1990, **67**, 829.
4 M. L. Occelli and H. C. Robson, *Zeolite Synthesis*, American Chemical Society, Washington, D.C., 1989.
5 C. T. Kresge, M. E. Leonowicz, W. J. Roth, J. C. Vartuli and J. S. Beck, *Nature* (*London*), 1997, **359**, 710.
6 M. I. Khan, L. M. Meyer, R. C. Haushalter, C. L. Schweitzer, J. Zubieta and J. L. Dye, *Chem. Mater.*, 1996, **8**, 43 and refs. therein.
7 S. Mann, S. L. Burkett, S. A. Davis, C. E. Fowler, N. H. Mendelson, S. D. Seins, D. Walsh and N. T. Whilton, *Chem. Mater.*, 1997, **9**, 2300 and refs. therein.
8 S. I. Stupp and P. V. Braun, *Science*, 1997, **277**, 1242 and refs. therein.
9 P. J. Hagrman, D. Hagrman and J. Zubieta, *Angew. Chem.*, *Int. Ed.*, 1999, **38**, 2638 and refs. therein.
10 D. Hagrman, C. Zubieta and D. J. Rose, J. Zubieta and R. C. Haushalter, *Angew. Chem.*, *Int. Ed. Engl.*, 1997, **36**, 873.
11 D. Hagrman, C. Sangregorio, C. J. O'Connor and J. Zubieta, *J. Chem. Soc.*, *Dalton Trans.*, 1998, 3707.
12 D. Hagrman, R. P. Hammond, R. Haushalter and J. Zubieta, *Chem. Mater.*, 1998, **10**, 2091.
13 D. Hagrman, C. J. Warren, R. C. Haushalter, C. Seip, C. J. O'Connor, R. S. Rarig, Jr., K. M. Johnson III, R. L. LaDuca, Jr. and J. Zubieta, *Chem. Mater.*, 1998, **10**, 3294.
14 D. Hagrman and J. Zubieta, *C. R. Acad. Sci. Paris*, *Ser. IIc*, in press.
15 D. Hagrman, P. Hagrman and J. Zubieta, *Inorg. Chim. Acta*, 2000, **300–302**, 212.
16 J. Fuchs, S. Mahjour and J. Pickardt, *Angew. Chem.*, *Int. Ed. Engl.*, 1976, **15**, 374.
17 M. C. Laskoski, R. L. LaDuca, Jr., R. S. Rarig, Jr. and J. Zubieta, *J. Chem. Soc.*, *Dalton Trans.*, 1999, 3467.
18 I. D. Brown, *J. Chem. Inf. Comput. Sci.*, 1989, **29**, 266.